Experimental Mechanics
DOI 10.1007/s11340-015-0119-9

A Method to Measure Moisture Induced Swelling Properties of a Single Wood Cell

T. Joffre[1] · P. Isaksson[1] · P.J.J. Dumont[2,3,4,8] · S.Rollanddu Roscoat[5,6,7] · S. Sticko[1] · L. Orgéas[5,6] · E.K. Gamstedt[1]

Received: 30 April 2015 / Accepted: 14 December 2015

Abstract Wood cells constitute the main building block in engineered wood-based materials, whose delimiting property frequently is moisture induced swelling. The hygroexpansion properties of wood cells, technically known as fibers, are used as input in predictive micromechanical models aimed for materials design. Values presented in the literature largely depend on the microfibrillar angle, the geometry of the fiber and limiting modelling assumptions. Synchrotron X-ray micro-computed tomography has recently prompted means for detailed measurements of the geometry of unconstrained individual fibers undergoing moisture-induced swelling, which makes it possible to directly quantify the hygroexpansion properties of the cell wall. In addition to a well-defined three-dimensional geometry, the present approach also accounts for large deformations and the fact that cell-wall stiffness depends on the presence of moisture. A mixed numerical-experimental approach is adopted where a finite-element updating scheme is used to simulate the swelling of an earlywood spruce fiber going from the experimental fiber geometry at 47 % relative humidity to the predicted geometry of the fiber in the wet state at 80 % relative humidity at equilibrium conditions. The hygroexpansion coefficients are identified by comparing the predicted and the experimental three-dimensional fiber geometry in the wet state. The obtained values are 0.17 strain per change in relative humidity transverse to the microfibrils in the cell wall, and 0.014 along the microfibrils.

Keywords Wood fiber · X-ray microtomography · Finite element method · Hygroexpansion

✉ E. K. Gamstedt
kristofer.gamstedt@angstrom.uu.se

[1] Department of Engineering Sciences, Ångström Laboratory, Uppsala University, Box 534, SE-751 21 Uppsala, Sweden

[2] Université Grenoble Alpes, LGP2, F-38000 Grenoble, France

[3] CNRS, LGP2, F-38000 Grenoble, France

[4] Agefpi, F-38400 Saint-Martin-d'Hères, France

[5] Université Grenoble Alpes, 3SR Lab, F-38000 Grenoble, France

[6] CNRS, 3SR Lab, F-38000 Grenoble, France

[7] ESRF, ID 19 Topography and Microtomography Group, 38043 Grenoble Cedex, France

[8] Present address: Université de Lyon, INSA-Lyon, LaMCoS CNRS UMR5259, F-69621 Villeurbanne Cedex, France

Introduction

The drive for renewable materials has prompted increased research for the use of natural cellulose fibers as reinforcement in composites [1–3] and the use of wood in structural members [4–6]. The use of renewable cellulose fibers, such as wood fibers, in structural materials is challenging because of their inherent hygroexpansion behavior caused by moisture absorption. Due to the abundance of hydroxyl groups present in a wood fiber, the fiber will inevitably take up water and swell in a moist environment. In predictive micromechanical models linking wood fiber hygroexpansion to the swelling of engineered wood-based materials, a necessary input is the hygroexpansion properties of the wood cell wall itself. Such micromechanical models could potentially be used in materials design, where the limiting factor in many cases is moisture-induced deformations. A weakest link in such models is frequently the material properties of the constituents. The hygroexpansion coefficients of the wood fiber or more specifically its cell wall is a crucial parameter, which is not straightforward to measure directly. The cell-wall hygroexpansion, intimately linked to the fiber swelling, has

Published online: 05 January 2016

been estimated from (i) the swelling behavior of the polymer constituents and ultrastructure (*cf*. [7–9]), measurements of solid wood (*e.g.*, [10]), or estimations from measurements of wood-fiber composites [11]. Recent development in synchrotron X-ray computed microtomography provides us with a powerful tool to measure dimensional changes *in situ* of minute material samples, such as wood fibers. By a combination of three-dimensional finite element analysis and three-dimensional imaging of single wood fibers under different states of equilibrium moisture contents, direct measurements of the cell-wall swelling properties can be achieved. This is the scope of the present work.

In order to relate the swelling of the cell-wall layers to that of a wood fiber, the geometry, ultrastructure and layer composition need to be quantified. The wood fiber wall consists of an assembly of several layers that show differences in their structure and chemical composition. The secondary fiber wall (S2 layer) forms the main part of the cell wall and thus has a large influence on the mechanical and physical properties of the fiber (see *e.g.*, [12]). The S2 layer exhibits a helical structure (see Fig. 1), where the cellulose microfibrils are wound around the axis of the fiber with an angle, known as the microfibril angle (MFA). The microfibrils are surrounded by a matrix of hemicelluloses and lignin. The helical structure of the main layer of the cell-wall implies that the fiber will twist if the moisture content changes [13, 14]. Given the significant observed twist in free fibers, the inclined hygroelastic anisotropy needs to be taken into consideration in a modelling approach. Due to the dominating relative significance of the S2 layer [7, 15], on the hygroelastic response of the fiber, only this layer was included in the present study.

Different modelling approaches have been used aiming to understand the hygroelastic behavior of wood [16–20]. Some experiments have been carried out to validate such theoretical approaches using direct measurement on wood sample [20], electron microscopy [21] or X-ray microtomography [22]. In wood, the fibers, or tracheids, are glued together by the middle lamella and the twist of the fiber is constrained by its neighbors. The relation between the cell-wall swelling and wood tissue swelling is affected by the constraining stress transfer between cells and the geometrical details of the wood microstructure. The unhindered cell-wall swelling of free-standing fibers would be more directly linked to the intrinsic swelling of the cell wall. In recent modelling work on hygroexpansion of single wood fibers (*e.g.*, [8, 23, 24]), there is a lack of reliable input data on the hygroexpansion of the main cell-wall layer or that of the constituent cell-wall polymers. Swelling tests of individual free fibers is cumbersome due to the small dimensions and irregular shape of the fibers. X-ray micro-computed tomography (XμCT) presents a three-dimensional imaging technique with a resolution high enough to capture microscopic swelling or shrinkage. To this end, XμCT has already been successfully used to characterize the microstructure of different engineering materials where wood fibers are used as structural framework, such as wood itself [22, 25, 26], cardboard [27], paper [28–32] or fiber reinforced polymer composite materials [33, 34]. With the high resolution obtained in XμCT at synchrotron facilities, such as the European Synchrotron Radiation Facility (ESRF), it has become possible to obtain high quality images of isolated natural fibers, in a relatively short time (of the order of minutes). The relatively short scanning time is a necessity to capture hygroscopically-induced shape changes in cellulosic fibers. Recent work on this subject includes the study by Rafsanjani et al. [35] who first used a focus ion beam to cut regular rectangular blocks in the cell wall and then microtomography to investigate the dimensional change due to moisture uptake. This innovative approach has the advantage of quantifying the swelling properties locally in the S2 layer from which the rectangular block was cut. In the present work, the swelling behavior of a whole tracheid was investigated. The irregular shape of the fiber is accounted for in the numerical

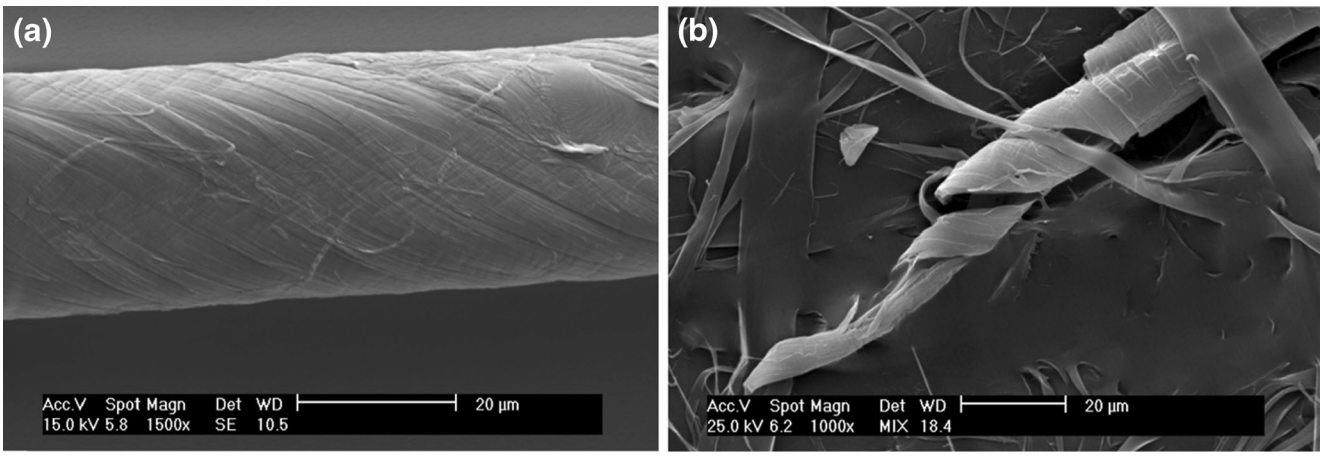

Fig. 1 Scanning-electron micrographs showing examples of the helical structure of a wood fiber: (**a**) a Norway spruce fiber in the green state, the microfibrils of cellulose are wound around the longitudinal axis of the fiber, and (**b**) a damaged spruce wood pulp fiber in paper revealing the helical structure of the fiber

calculations to obtain the cell-wall properties. The fiber was isolated and treated with care, to maintain its properties in the native green state, thus avoiding any possible effects from mechanical or ion beam cutting. The captured geometries can then be used in numerical simulations to identify the cell-wall hygroelastic properties. The hygroexpansion parameters must then be identified by an inverse method. A rather comprehensive review of such mixed numerical-experimental techniques has been compiled by Avril et al. [36]. Some applications in wood mechanics has been outlined by Gamstedt et al. [37].

In this study, a finite element model updating scheme is applied to the deformation of a complex shaped wood obtained by the means of XμCT. The general idea is presented in Fig. 2: XμCT is used to determine the geometry of an isolated wood tracheid at two different ambient relative humidities. The obtained geometry is then used as input of a finite element simulation. The hygroexpansion coefficients used in the finite element model were updated to have the numerical deformation matching the experimental one. As a result, it was possible to obtain the hygroexpansion coefficient of a single wood fiber in both the direction transverse to the fibrils and the direction longitudinal to the fibrils. The swelling of fiber might be regarded as a structural property since it depends on some variable parameters such as the MFA, the geometry of the fiber and the thickness of the cell wall, which are likely to vary from fiber to fiber in any wood sample. The hygroexpansion coefficients of the cell-wall layer (essentially the S2 layer) measured here should be independent on the aforementioned parameters, and might thus be regarded as material properties. It should be noted that the preparation and scanning processes are time consuming for materials such as single wood fibers. With the limitation in beam time, only one fiber could therefore be scanned. Since different factors, such as the sample preparation or the variability of wood properties across the growth rings, could affect the swelling properties, it is not possible to conclude on whether or not theses values could be regarded as material properties for spruce earlywood fibers. Before scanning, the morphology of the selected fiber was carefully investigated in a microscope and compared with other fibers from spruce wood samples, to confirm that the chosen fiber was structurally representative. However, in the future more experiments should be carried out to give improved statistical material and strengthen the strategy used.

Experimental Procedures

Materials and X-ray Micro-Computed Tomography

Wet never dried earlywood tracheids were extracted from a stem of Norway spruce (*Picea Abies*) using thin tweezers. Limitations in beam time and computational resources confined us to analyze only one earlywood fiber fully. Before scanning, the morphology of the selected fiber was carefully investigated under microscope and compared with other fibers from spruce wood samples, to confirm that chosen fiber was structurally representative. After the scanning the twist of other fibers were also observed under magnification, and showed the same general behavior as the fiber analyzed in detail by XμCT. The fiber was extracted imminently before the scans. The scans were performed at two different levels of relative humidity (RH): 47 %, which corresponds to the ambient RH, and will be referred to as the dry state, and 80 % RH which will be referred to as the wet state. The relative humidity was controlled by a gentle flow of air at 80 % RH inside the Plexiglas pipe where the fiber was located. During the scanning time, the pipe was sealed to minimize fiber motion, and the air was blown all around the Plexiglas pipe to keep the surrounding climate at a constant temperature and relative humidity (see Fig. 3). Equilibrium conditions were achieved almost instantaneously due to the small dimensions of the fiber and the scans were performed approximatively 10 min after the desired relative humidity had been reached. To mount the sample, one end of the fiber was embedded in an epoxy adhesive. The epoxy adhesive can slightly constrain the radial swelling of the fiber in its vicinity. To minimize this effect the

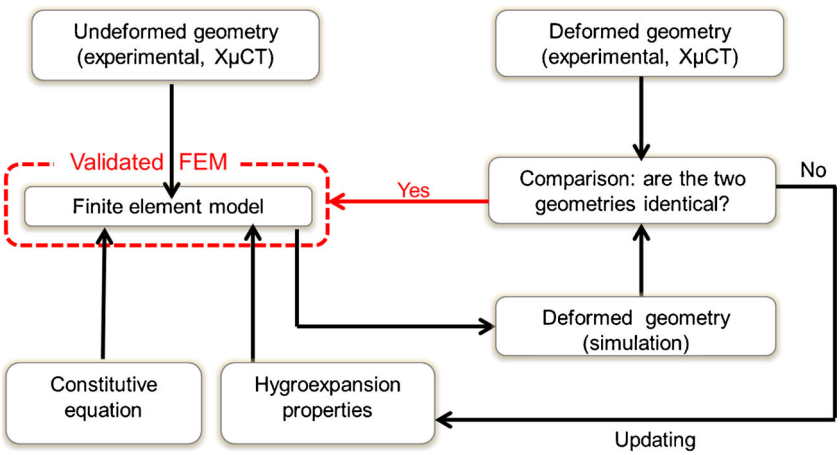

Fig. 2 Approach developed in the present study

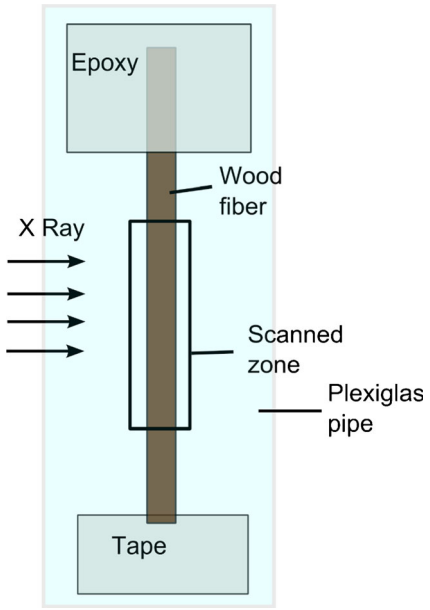

Fig. 3 Schematic drawing showing the experimental setup. The adhesive tape was removed when the relative humidity was changed

fiber was not studied anywhere close to the epoxy droplet. The other extremity was loosely attached to the edge of an adhesive tape, such that it could be removed when the relative humidly was changed, and held in place during the scanning time to avoid any excessive movement of the fiber. The stabilization of the adhesive tape and protective pipe was necessary to achieve sufficiently high image quality. Absorption tests were performed, going from equilibrium conditions at 47 % RH to 80 % RH. Note that below 80 % of RH the moisture is mainly absorbed by the cell wall, where unbound water adsorbed on lumen surfaces appears at higher relative humidity level [15]. In principle, the moisture content of the cell wall would be a better physical measure than the ambient relative humidity, but the mass of the fiber is too low to be measured accurately. Although the sorption isotherm is known to be non-linear for wood [38], it was considered that the experiments were carried out in a linear regime between the far from completely drying the fiber out and fiber saturation point. It was thus assumed that moisture uptake of the cell wall is proportional to the change in RH. The hysteresis of the sorption isotherm implies that the absorption and desorption must be distinguished (see *e.g.*, [25, 39]). Only absorption, relevant to dimensional instability of swelling wood materials, was considered here.

The images were obtained by taking 1500 radiographs (acquisition time of 0.2 s for each) over 180° of the single fiber at each relative humidity step on the beamline ID19 of the ESRF (Grenoble, France). The fiber was irradiated by an X-ray monochromatic beam light (energy E=17.6 keV; $\Delta E/E=2\times 10^{-5}$). The transmitted light was converted into visible light using a GGG ($Gd_3Ga_5O_{12}$) 6 μm scintillator and recorded using the FReLoN camera at ESRF. The combination of the used equipment gave a pixel size of 0.35 μm in the projected 2D images. The 3D images were reconstructed using a filter-back projection algorithm [40].

Microfibril Angle Measurement

The anisotropy of the cell wall is essentially controlled by the direction of the microfibrils in the cell wall. This value is used as an input to the numerical model. The microfibrils within the cell wall are highly crystalline and aligned in the different layers, S1, S2 and S3 [41]. As a result of the molecular orientation, the birefringence clearly manifests itself when a thin section of wood is analyzed in optical microscopy between two crossed polarizing filters. This phenomenon has been widely used to measure the average MFA of the cell wall [42–44]. Because of the helical orientation of the fibrils (see Fig. 1), only one cell wall has to be in the path of the light to measure the MFA accurately. Thus in the present work, the extremity of the fiber was sectioned longitudinally with a thin razor blade. Then the fiber was rotated between two cross polarizing filters to find the angle where no light is able to go through the cell wall. This position is called the maximum extinction position (MEP). The average MFA of the cell wall corresponds to the angle between the fiber axis and the MEP. It should be highlighted that the obtained value corresponds to the weight average through the cell wall [45]. However, the influence of P, S1 and S3 layers are in most cases negligible, since the S2 layer is much more thicker and constitutes 90 % of the cell wall [46]. For the same reasons, only the S2 layer was included in numerical analysis. The MFA was measured on the same fiber as the one subsequently analyzed by XμCT.

Image Processing

A median filter, with a 3×3×3 mask, was applied to smooth and remove the background noise of the images. The images were then thresholded using a value determined manually. Since the synchrotron images had a very high contrast, the threshold level did not have a large impact on the obtained thickness values of the cell wall. In order to facilitate the meshing procedure the edges of the image were smoothed. This was carried out using morphological opening [47] with a radius of 5 voxels. The image processing is exemplified in Fig. 4. Sometimes small thin sections that were considered as sublayers from adjacent tracheids were found in the images, as shown in Fig. 4(a) and (b). The adhering leaflets from adjacent tracheids were assumed not to influence the global hygroexpansion of the analyzed fiber. However, they were used as markers to ensure that the same part of the fiber was analyzed in the dry and in the wet state. Since the fiber was moving as the relative humidity was changed, it was necessary to find a unique reference point on the cell wall which was tracked through the deformation for purpose of relocation.

Fig. 4 Cross-section of a fiber (**a**) before any image processing, (**b**) after thresholding, and (**c**) after morphological opening

Modelling the Hygroelastic Behavior of a Wood Fiber

Constitutive Model

Two coordinate systems, a global Cartesian (X_1,X_2,X_3) and a local curved polar (r,θ,z), are introduced as illustrated in Fig. 5. The global coordinate directions are such that X_3 coincides with the principal fiber direction. The helical fiber structure is assumed to curl around X_3 along the fiber, and for simplicity, it is further assumed that the MFA φ is constant along the whole fiber (see Fig. 5) meaning that any variable transformation between the two coordinate systems becomes quite simple. Müller et al. [48] used X-ray diffraction on a single wood fiber and observed only very small variation in MFA inside the same fiber. We assumed that the MFA was constant throughout our fiber as well. A variation in RH from 47 to 80 % should result in a variation of MFA of less than one degree [13], and since this limited variation was close to the measurement error, the MFA was simply considered to be constant in the simulations. Due to the severe moisture induced swelling of the fiber that took place, both large deformations and rotations were included in the analysis. In the current deformed configuration, the position vector $\boldsymbol{X}$ refers to a position in the body in a fixed reference configuration and $\boldsymbol{x}$ denotes the position vector to the same point in the deformed configuration. Both $\boldsymbol{X}$ and $\boldsymbol{x}$ are described in a Cartesian coordinate system. A fundamental measure of deformation is described by the deformation gradient given by

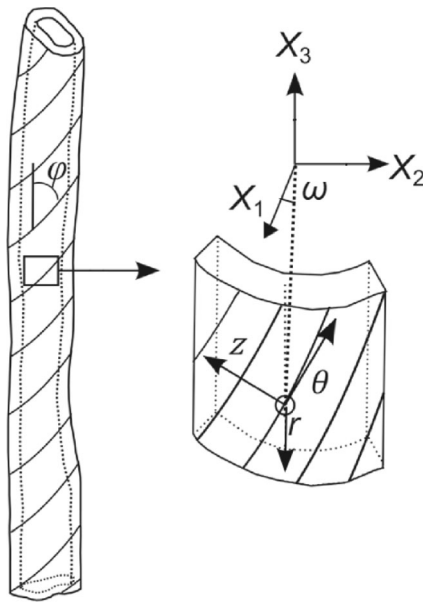

Fig. 5 Global (X_1, X_2, X_3) and local (r, θ, z) coordinate system, where φ represents the MFA

$$\boldsymbol{F} = \frac{\mathrm{d}\boldsymbol{x}}{\mathrm{d}\boldsymbol{X}} \tag{1}$$

The change in volume of a material element between its reference and current configuration is given by $\mathrm{d}V = \boldsymbol{J}\mathrm{d}V_0 = \det(\boldsymbol{F})\mathrm{d}V_0$. Because of the physical constraint that the volume cannot obtain negative values, $\boldsymbol{J}$ is subjected to the condition $\boldsymbol{J} = \det(\boldsymbol{F}) > 0$. More details to this topic can be found in the literature (*cf.* [49–51]). A Lagrangian formulation is applied and an assumption that the body admits the right Cauchy-Green strain tensor $\boldsymbol{C}$ given by

$$\boldsymbol{C} = \boldsymbol{F}^{\mathrm{T}}\boldsymbol{F}, \tag{2}$$

is made. Further, assume the humidity $\boldsymbol{\eta}$ and $\boldsymbol{C}$ are independent mechanical variables. Suppose further the existence of a Helmholtz free energy function in the form of $\psi = \psi(\boldsymbol{C}, \boldsymbol{\eta})$ (*cf.* [52]). The conjugated second Piola-Kirchhoff stress $\boldsymbol{S}$ of a point at a certain load is then a nonlinear tensor of the two variables $\boldsymbol{C}$ and $\boldsymbol{\eta}$, *i.e.*, $S = S(\boldsymbol{C}, \boldsymbol{\eta})$. The stress increment $\mathrm{d}\boldsymbol{S}$ is then obtained by taking the differential of the stress $\boldsymbol{S}$ according to [52]

$$\mathrm{d}\boldsymbol{S} = \boldsymbol{D} : \frac{1}{2}\mathrm{d}\boldsymbol{C} + \boldsymbol{B} : \mathrm{d}\boldsymbol{\eta}, \text{ where} \tag{3}$$

$$\boldsymbol{D} = 2\frac{\partial \boldsymbol{S}(\boldsymbol{C}, \boldsymbol{\eta})}{\partial \boldsymbol{C}} d\boldsymbol{C} = 4\frac{\partial^2 \psi(\boldsymbol{C}, \boldsymbol{\eta})}{\partial \boldsymbol{C}\partial \boldsymbol{C}} \text{ and} \tag{4}$$

$$\boldsymbol{B} = \frac{\partial \boldsymbol{S}(\boldsymbol{C}, \boldsymbol{\eta})}{\partial \boldsymbol{\eta}} = 2\frac{\partial^2 \psi(\boldsymbol{C}, \boldsymbol{\eta})}{\partial \boldsymbol{C}\partial \boldsymbol{\eta}} \tag{5}$$

is the elasticity stiffness tensor and the stress-humidity tensor, respectively. Both tensors are symmetric, $\boldsymbol{D}$ of rank 4 while $\boldsymbol{B}$ has rank 2. The stress increment $\mathrm{d}\boldsymbol{S}$ thus measures the change in stress that results from a change in strain or humidity,

respectively. The updated second Piola-Kirchhoff stress after humidity change d$\boldsymbol{\eta}$ during a time Δt, from t to $t+\Delta t$, using (3), becomes

$$^{t+\Delta t}\boldsymbol{S} = {}^{t}\boldsymbol{S} + \mathrm{d}\boldsymbol{S} = {}^{t}\boldsymbol{S} + {}^{t}\boldsymbol{D} : \frac{1}{2}\mathrm{d}\boldsymbol{C} + {}^{t}\boldsymbol{B} : \mathrm{d}\boldsymbol{\eta} \tag{6}$$

For processes involving change of humidity $\boldsymbol{\eta}$ the volume might change (*cf.* [53]). This is here accounted for using the Cauchy stress $\boldsymbol{\sigma}$, which measures the stress in the current configuration and is obtained from a Piola transformation of $\boldsymbol{S}$ (*cf.* [52, 54]). The current updated Cauchy stress, after humidity change d$\boldsymbol{\eta}$, becomes

$$^{t+\Delta t}\boldsymbol{\sigma} = \boldsymbol{J}^{-1}\boldsymbol{F}\boldsymbol{S}\boldsymbol{F}^{T}{}_{t+\Delta t} \tag{7}$$

In equation (4), it is assumed that the tensors $\boldsymbol{D}$ and $\boldsymbol{B}$ are constant within each small humidity increment d$\boldsymbol{\eta}$. Moreover, the tensors $\boldsymbol{D}$ and $\boldsymbol{B}$ are given in the global Cartesian coordinate system (X_1,X_2,X_3), while the material properties of the fiber are given in the local polar coordinate system (r,θ,z) wherefore appropriate rotations have to be made.

The global stiffness matrix is obtained by two straightforward transformations. First, the elastic stiffness tensor, $\boldsymbol{E}$, of the cell wall in local coordinates (r,θ,z), with θ being the fibril direction, is rotated with an angle φ to the cylindrical coordinate system, $\tilde{\boldsymbol{E}}=\boldsymbol{T}\boldsymbol{E}\boldsymbol{T}^{T}$, and then rotated once again an angle ω (as shown in Fig. 5) to the global Cartesian coordinate system (X_1,X_2,X_3),$\boldsymbol{D}=\boldsymbol{L}^{-1}\tilde{\boldsymbol{E}}\boldsymbol{L}^{-T}$. The rotation matrices [$\boldsymbol{L}$] and [$\boldsymbol{T}$] are given and illustrated in Appendix A. The cell wall can be assumed transversely isotropic normal to the direction of the fibrils [55]. The stiffness tensor $\boldsymbol{C}$ used in this study has been calculated from the elastic properties of the wood polymers and is given as a function of the relative humidity in Appendix B. The stiffness tensor is updated after each small humidity increment d$\boldsymbol{\eta}$. The stress-humidity tensor is given by $\boldsymbol{B}=\boldsymbol{L}^{-1}\boldsymbol{T}\boldsymbol{E}\boldsymbol{\beta}$, where $\boldsymbol{\beta}$ is the hygroexpansion coefficient expressed in the local coordinate system (r,θ,z). The hygroexpansion coefficient is assumed to be transversely isotropic in the fibril direction, *i.e.*, $\boldsymbol{\beta} = \{\,\beta_T,\quad \beta_L,\quad \beta_T,\quad 0,\quad 0,\quad 0\,\}^{\boldsymbol{T}}$ in the local coordinate system.

Numerical Method

The finite element calculations were carried out in a Matlab (2015) code. A 3D isoparametric solid material 8-node element, with three nodal degrees of freedom *i.e.*, translation in X_1, X_2 and X_3-directions, were used. The model consisted of around 4000 elements. The element formulations were capable of handling large strains and rotations, and followed standard implementation algorithms found in *e.g.*, Bathe [49] or Crisfield et al. [50]. A total Lagrange formulation is the basis for all kinematic relations. Appropriate stress and deformation measures were obtained as described in the previous section. A Newton–Raphson iteration scheme for the solution of nonlinear finite-element equations is employed in all time steps. The governing quasi-static equations were

$${}^{t}\mathbf{K}\Delta\mathbf{U}^{(i)} = {}^{t+\Delta t}\mathbf{R} - {}^{t+\Delta t}\mathbf{F}^{(i-1)} \tag{8}$$

$${}^{t+\Delta t}\mathbf{U}^{(i)} = {}^{t+\Delta t}\mathbf{U}^{(i-1)} + \Delta\mathbf{U}^{(i)} \tag{9}$$

where ${}^{t}\mathbf{K}$ is the stiffness matrix at time t, ${}^{t+\Delta t}\mathbf{R}$ is a load vector representing the driving forces including the body and surface forces at time $t+\Delta t$, ${}^{t+\Delta t}\mathbf{F}^{(i-1)}$ is the nodal force vector corresponding to the elements stresses due to the displacement vector ${}^{t+\Delta t}\mathbf{U}^{(i-1)}$. The superscript i denotes the iteration number and the vector $\Delta\mathbf{U}^{(i)}$ represents the increment in the nodal displacement at iteration i. It is noted that the load vector $\mathbf{R}$ in equation (8) was included for the sake of completeness. In the present study there are no externally applied loads, and $\boldsymbol{R}=\boldsymbol{0}$ at all times. The incremental nonlinear Green deformation tensor d$\boldsymbol{C}$ in (4) was continuously updated at every Newton-iteration until Cauchy stress equilibrium, equation (7), prevailed everywhere in the body and the solved displacements ${}^{t+\Delta t}\mathbf{U}^{(i)}$were obtained. It is underlined that all deformations originated entirely from a humidity change d$\boldsymbol{\eta}$ in (4) and the consequence of stress equilibrium.

Meshing

The 3D image obtained in the reference configuration (47 % RH) was used as a framework for building a mesh with 8-node volume elements. The meshing technique was adapted for slender hollow irregular twisted tubes such as wood fibers. The core of the method consisted of (i) determining the cross section of the slender object, (ii) detecting the curves that formed their inner and outer boundaries, as shown in Fig. 6(a), and (iii) fitting an ellipsoid to determine the starting points for the meshing. These operations were followed by constructing layers of nodes from the inner and outer curves, as illustrated in Fig. 6(b). Since the inner and outer boundaries were detected from thresholded images, the initial mesh (*cf.* Fig. 6(c)) was edgy with a step size given by the scanning resolution. To get around this, the mesh was smoothed first in the horizontal and then in the vertical direction. Horizontally, the points on the inner and outer boundaries were smoothed using quadratic local regression [56]. The mesh was then smoothed in the vertical direction by applying quadratic local regression to each set of mesh nodes connected in the vertical direction. The layers of nodes were then connected to form a smooth mesh, as can be seen in Fig. 6(c).

Around 4000 hexahedral elements were created in this way.

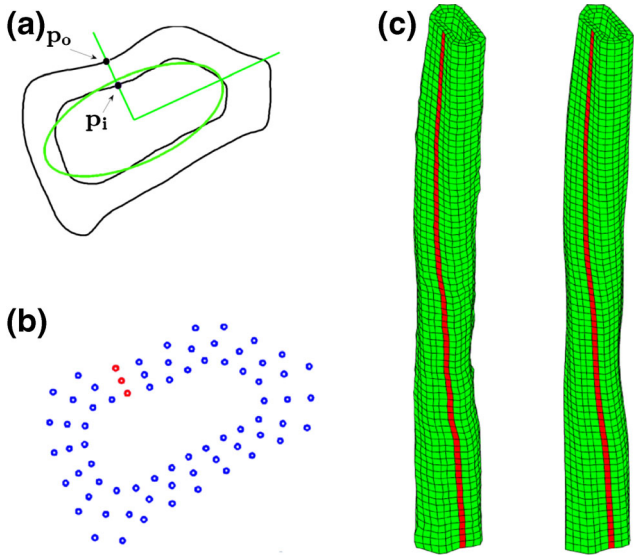

Fig. 6 Illustration of the meshing process of a 3D image of a wood fiber obtained using X-ray microtomography: (**a**) Detection of the inner and outer contours of the fiber cross sections, and fitting of an ellipsoid to find the starting points (p_o and p_i) of the meshing procedure. (**b**) Repartition of the FEM mesh nodes in a fiber cross section. (**c**) Illustration of the complete finite-element mesh built from the X-ray image before (*left*) and after (*right*) smoothing operation. The length of the fiber is approximately 300 μm. The *red line* is used to follow the twist of the fiber

Boundary Conditions

To capture the relatively large rotations and deformations induced by the swelling mechanism observed in experiments, two nodes of the first external layer were clamped at one end of the fiber while the rest of the nodes of this layer were freely able to move in the X_1-X_2 plane. The rest of structure was unconstrained. Using these boundary conditions, the rotation of the first layer was constrained without significantly affecting the global swelling behavior of the fiber, since less than 0.1 % of the fiber was constrained in this way. In the experiment the fiber was also rotating between the fixation and the segment considered in the numerical simulation (see Fig. 3). As a result there was a difference of orientation between the first layer of the model and the first slice of the experiment. To compare the experimental and numerical results it was thus necessary to account for a rigid body motion, which was done by rotating the original image around the X_3 axis in order to align both orientations.

Simulation and Updating of the Material Properties

First the meshing procedure described in the previous section was applied to the scan of the wet fiber (80 % RH), in order to avoid any bias due to irreversible operation such as smoothing or morphological opening used during the meshing process. Then the fiber geometry resulting from the finite-element simulation of the wet fiber was compared with this mesh of the scanned wet fiber. To quantify the distance between the geometry of the simulation and the measurement, three different measures were defined as the difference of (i) the volume of the fibers which was computed as the sum of the volume of each element (ii), the length of the fibers which was approximated by adding the distance between the mass center of all the elements within one layer of node, and (iii) the twist of the fibers which was taken as the difference of angle between the main direction of the ellipsoids fitted to the first and last layer of node.

The inverse problem then consisted in identifying the hygroexpansion coefficients β_L and β_T which minimized the distance difference between the two meshes, d, expressed as

$$d = \left(\frac{|\Delta\theta|}{\Delta\theta_{exp}}\right)^2 + \left(\frac{|\Delta L|}{\Delta L_{exp}}\right)^2 + \left(\frac{|\Delta V|}{\Delta V_{exp}}\right)^2 \quad (9)$$

where $\Delta\theta$, ΔL and ΔV are the variation of angle, length and volume between the numerical and experimental meshes, normalized with $\Delta\theta_{exp}$, ΔL_{exp} and ΔV_{exp}, corresponding to the difference between the two experimental geometries for 47 and 80 % RH. Figure 7 summarizes the updating procedure used in this study. The minimization was performed using the built-in 'fminsearch' function in Matlab and no particular weights was given to the different parts in equation (9). The initial values for the hygroexpansion coefficient were taken from litterature [14] and constrained to positive values. The experimental change in RH was simulated from 47 to 80 % using an increment dR (see equation 4) equal to 1 % RH. This step size was found to be sufficiently small in solving the initial value problem.

Results and Discussion

The microfibril angle for spruce fiber studied was found to be 15° by optical microscopy with transmitted light through cross polarized filters. The mixed numerical-experimental approach described above was used to calculate hygroexpansion coefficient of the cell wall. The results are presented in Table 1, together with values reported elsewhere. A three-dimensional visualization of the studied fiber is shown in Fig. 8.

The obtained value for the transverse hygroexpansion coefficient fall in the lower part of the range 0.1-0.4 supported by other investigations such as estimation from sorption tests of composites [11], paper [57], and wood [10] or measurement on pulp fiber by means of X-ray microtomography [58]. However, it should be highlighted that the hygroexpansion was here measured in the direction of the fibrils, whereas all the aforementioned studies dealt with an average of the swelling of different fibers having different geometries as well as

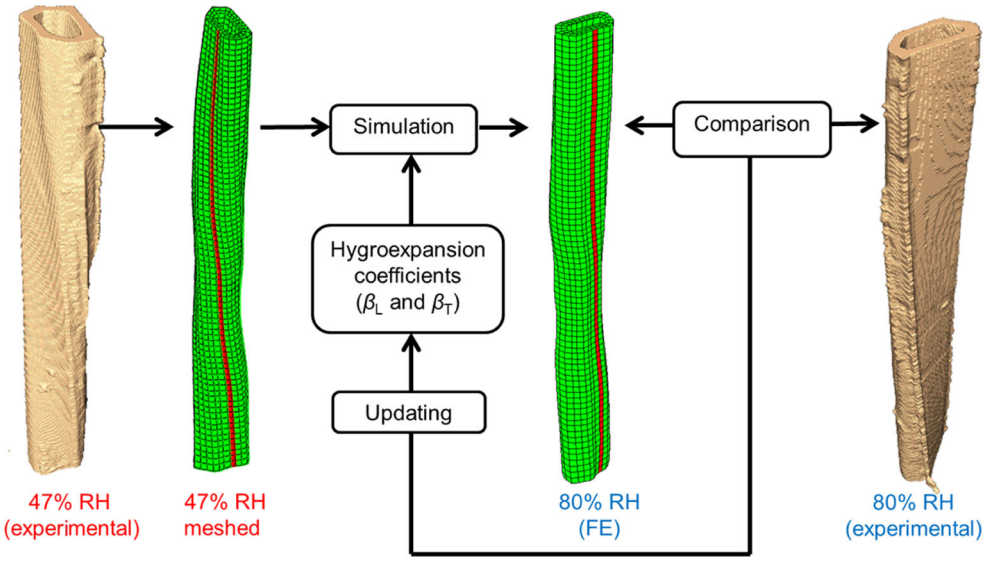

Fig. 7 Scheme of the finite-element updating approach used in the present study

different MFA. In processed fibers, such as pulp fibers, the cellulose ultrastructure is modified [59], and as a result the mobility of the polymer chains within the cell wall is affected, which impacts the hygroelastic properties. The micromechanical models in Table 1 are based on different sets of assumptions. The assumptions in the present model are considered to be more realistic and less constraining than those in the other approaches. The advantages of the present approach are that (i) the detailed geometry of the fibers is taken into account, (ii) large deformations and rotations are considered, (iii) the transverse and longitudinal hygroexpansion coefficients are identified independently, (iv) the moisture dependency of the elastic properties is represented.

As expected the longitudinal hygroexpansion coefficient is one order of magnitude lower than the transverse one. This is due to the orientation of the wood polymers within the cell wall: the hemicelluloses do not significantly swell in the longitudinal direction due to the relative rigidity of the aligned cellulose microfibrils [15]. Thus the swelling in the direction of the cellulose fibrils is significantly lower than that in the transverse direction. The β_L/β_T roughly equals that of the of the E_L/E_T ratio, which has also been found in previous studies [60, 61]. This indicates that compliance and swelling induced by moisture uptake in the considered hydrophilic polymers are related. The underlying molecular mechanism is that breakage of hydrogen bond of hydroxyl groups by water molecule induces both expansion and reduction in stiffness [62]. The values measured here are given as a strain per change in relative humidity. Using sorption isotherm of spruce earlywood [63], it is possible to convert these values as a strain per change in moisture content. Thus, the values reported here become 0.45 for β_T and 0.037 for β_L strain per change in moisture content.

We believe that the obtained values of the hygroexpansion coefficients obtained of a never dried Norway spruce fiber can in principle be regarded as material property to a larger degree than other reported values, since the values are obtained directly from a free-standing individual fiber and that the necessary assumptions are physically justified, namely the irregular fiber geometry, large deformations and microfibril angle are accounted for. It is therefore expected that the values could be used as input when modelling hygroexpansion of wood and

Table 1 Hygroexpansion coefficient estimated here and value from literature

Method	β_L (ε/RH)	β_T (ε/RH)
Identified from X-μCT and FE simulation (green state), this study	0.014	0.17
Back calculated from composite properties (pulp fibers)[a]		0.28
Measured from X-μCT images (pulp fibers)[b]		0.3
Measured from X-μCT images (wood)[c]		0.22
Estimated from paper sample[d]		0.17
Estimated from wood samples[e]		0.21
Estimated from FE simulation[f]		0.13
Analytical modelling based from input obtained by molecular dynamic simulation of the cell-wall polymers[g]	0.02	0.44

References: (a) [64] (b) [58] (c) [35] (d) [57] (e) [10] (f) [9] (g) [14]

Fig. 8 Three-dimensional view of a fiber at ambient relative humidity obtained by XμCT (length of the imaged zone of the fiber is 0.6 mm and the diameter is approximately 25 μm)

wood-based materials, provided that the cell-wall has a similar composition and ultrastructure.

Conclusions

A never dry cellulosic wood fiber was scanned in synchrotron X-ray micro-computed tomography under equilibrium conditions at two different levels of relative humidity. The obtained images were then used as input geometry in a three-dimensional finite element simulation. A mixed numerical-experimental method was used to identify the hygroelastic deformation of the wood fiber such that the numerical simulation matched the experimental results. Using this method it was possible to measure the hygroexpansion coefficients of an anisotropic irregular structure having a cross section smaller than 40 μm. The obtained values were 0.014 strain per change in relative humidity in the microfibril direction of the cell wall, and 0.17 in the transverse direction. Whereas the swelling of wood fiber depends on external parameters such as the microfibril angle and the geometry of the fiber, the method described here allows us to estimate coefficients independent of theses parameters. These coefficients can thus be used as inputs for models aiming to predict the hygroelastic behaviour of wood-fiber based engineering materials.

Acknowledgments The authors wish to thank Dr. Stig L. Bardage at SP Technical Research Institute of Sweden, for the electron microscopy images.

The authors from Uppsala are thankful for the financial support from the Swedish Research council Formas (grant 232-2014-202) and from EU COST Action FP0802 (Experimental and Computational Micro Characterization Techniques in Wood Mechanics).

The authors would also like to gratefully acknowledge the ESRF (beamline ID19) where the microtomography experiments were performed in the framework of the Long Term Project "ma127: Heterogeneous Fibrous Materials". This research was made possible at LGP2 thanks to the facilities of the TekLiCell platform funded by the Région Rhône-Alpes (ERDF: European Regional Development Fund). LGP2 and 3SR laboratories are parts of the LabEx Tec 21 (Investissements d'Avenir - grant agreement n°ANR-11-LABX-0030) and of the Énergies du Futur and PolyNat Carnot Institutes (Investissements d'Avenir - grant agreements n°ANR-11-CARN-007-01 and ANR-11-CARN-030-01).

Appendix A – Coordinate Transformation

Coordinate Transformation

The rotation tensor around X_3 axis is given on matrix form given by:

$$\boldsymbol{L} = \begin{bmatrix} c^2 & s^2 & 0 & 2cs & 0 & 0 \\ s^2 & c^2 & 0 & -2cs & 0 & 0 \\ 0 & 0 & 1 & 0 & 0 & 0 \\ -cs & cs & 0 & c^2-s^2 & 0 & 0 \\ 0 & 0 & 0 & 0 & c & -s \\ 0 & 0 & 0 & 0 & s & c \end{bmatrix} \tag{A1}$$

where ω is the angle between the X_1 axis and the r axis, $c = \cos\omega$ and $s = \sin\omega$. The rotation matrix around the r axis to account for the MFA is given by:

$$\boldsymbol{T} = \begin{bmatrix} 1 & 0 & 0 & 0 & 0 & 0 \\ 0 & C^2 & S^2 & 2CS & 0 & 0 \\ 0 & S^2 & C^2 & -2CS & 0 & 0 \\ 0 & 0 & 0 & 0 & S & C \\ 0 & -CS & CS & C^2-S^2 & 0 & 0 \\ 0 & 0 & 0 & 0 & C & S \end{bmatrix} \tag{A2}$$

were $C = \cos\varphi$ and $S = \sin\varphi$. The effects of the rotations on the reference coordinate system are illustrated in Fig. 9.

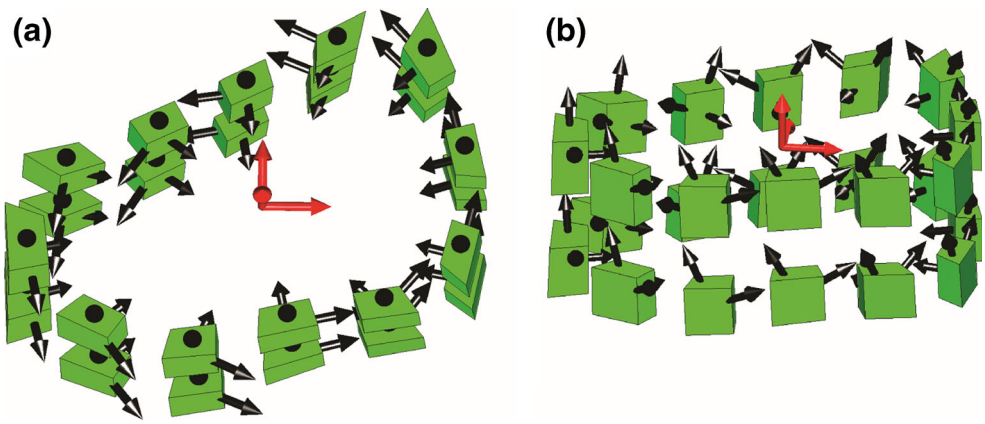

Fig. 9 Effects of the rotations on the reference coordinate system (*in red*) (**a**) Orientation after the first rotation around X_3, (**b**) rotation to account for the microfibril angle

Appendix B – Elastic Tensor

The material stiffness tensor E_{ijkl} (in the local coordinate system) used in the model was obtained from the properties and volume fraction of lignin, hemicellulose and cellulose using a composite micromechanical model at different levels of relative humidity as described by Joffre et al. [8]. The stiffness tensor E_{ijkl} was calculated as a function of the relative humidity from the engineering constants given in Table 2. For simulation purposes, a linear interpolation was used for approximating intermediate states.

Table 2 Elastic properties of the cell wall as a function of the moisture uptake in the longitudinal (L) and transverse (T) direction

RH %	E_L (GPa)	E_T (GPa)	G_{LT} (GPa)	G_{TT} (GPa)	V_{LT}	V_{TT}
10	72.5	8.69	2.75	3.02	0.44	0.19
20	72.3	8.30	2.64	2.89	0.44	0.19
30	72.0	7.83	2.51	2.73	0.43	0.19
40	71.6	7.31	2.36	2.55	0.43	0.19
50	71.3	6.73	2.19	2.36	0.43	0.19
60	71.0	6.08	2.01	2.14	0.42	0.19
70	70.5	5.26	1.76	1.86	0.42	0.19
80	70.0	3.87	1.33	1.38	0.40	0.19
90	69.3	1.42	0.53	0.52	0.38	0.20

References

1. Faruk O, Bledzki AK, Fink H-P, Sain M (2012) Biocomposites reinforced with natural fibers: 2000–2010. Prog Polym Sci 37: 1552–1596
2. La Mantia F, Morreale M (2011) Green composites: a brief review. Compos Part A 42:579–588
3. Mamun AA, Bledzki AK (2013) Micro fibre reinforced PLA and PP composites: Enzyme modification, mechanical and thermal properties. Compos Sci Technol 78:10–17
4. Dagenais C, Gagnon S, Desjardins R (2013) Performance-based design for mid-rise wood constructions in Canada. In: Cruz PJS (ed) Proceedings of the second international conference on structures and architecture: new concepts, applications and challenges. Taylor and Francis Group, London, pp 140–147
5. Li Z, He M, Lam F, Li M, Ma R, Ma Z (2013) Finite element modeling and parametric analysis of timber–steel hybrid structures. Struct Des Tall Special Build 23:1045–1063
6. van de Lindt JW, Pei S, Pryor SE, Shimizu H, Isoda H (2010) Experimental seismic response of a full-scale six-story light-frame wood building. J Struct Eng 136:1262–1272
7. Cave I (1972) A theory of the shrinkage of wood. Wood Sci Technol 6:284–292
8. Joffre T, Neagu RC, Bardage SL, Gamstedt EK (2014) Modelling of the hygroelastic behaviour of normal and compression wood tracheids. J Struct Biol 185:89–98
9. Persson K (2000) Doctoral thesis, micromechanical modelling of wood and fibre properties, division of structural mechanics. Lund Institute of Technology
10. Wallström L, Lindberg KAH (1999) Measurement of cell wall penetration in wood of water-based chemicals using SEM/EDS and STEM/EDS technique. Wood Sci Technol 33:111–122
11. Almgren KM, Gamstedt EK, Varna J (2010) Contribution of wood fiber hygroexpansion to moisture induced thickness swelling of composite plates. Polym Compos 31:762–771
12. Barnett J, Bonham VA (2004) Cellulose microfibril angle in the cell wall of wood fibres. Biol Rev 79:461–472
13. Burgert I, Frühmann K, Keckes J, Fratzl P, Stanzl-Tschegg S (2005) Properties of chemically and mechanically isolated fibres of spruce (Picea abies [L.] Karst.). Part 2: twisting phenomena. Holzforschung 59:247–251
14. Neagu RC, Gamstedt EK (2007) Modelling of effects of ultrastructural morphology on the hygroelastic properties of wood fibres. J Mater Sci 42:10254–10274
15. Cave I (1978) Modelling moisture-related mechanical properties of wood part i: properties of the wood constituents. Wood Sci Technol 12:75–86
16. Hassani MM, Wittel FK, Hering S, Herrmann HJ (2015) Rheological model for wood. Comput Methods Appl Mech Eng 283:1032–1060
17. Qing H, Mishnaevsky L (2009) Moisture-related mechanical properties of softwood: 3D micromechanical modeling. Comput Mater Sci 46:310–320
18. Rafsanjani A, Lanvermann C, Niemz P, Carmeliet J, Derome D (2013) Multiscale analysis of free swelling of Norway spruce. Compos Part A 54:70–78
19. Wang N, Liu W, Lai J (2014) An attempt to model the influence of gradual transition between cell wall layers on cell wall hygroelastic properties. J Mater Sci 49:1984–1993
20. Yamamoto H, Sassus F, Ninomiya M, Gril J (2001) A model of anisotropic swelling and shrinking process of wood. Wood Sci Technol 35:167–181
21. Keckes PF, Stanzl-Tschegg S (2005) Properties of chemically and mechanically isolated fibres of spruce (Picea abies wL. x Karst.). Part 2: twisting phenomena. Holzforschung 59: 247–251
22. Badel E, Perré P (2001) Using a digital X-ray imaging device to measure the swelling coefficients of a group of wood cells. NDT E Int 34: 345–353
23. Burgert I, Eder M, Gierlinger N, Fratzl P (2007) Tensile and compressive stresses in tracheids are induced by swelling based on geometrical constraints of the wood cell. Planta 226:981–987
24. Marklund E, Varna J (2009) Modeling the hygroexpansion of aligned wood fiber composites. Compos Sci Technol 69:1108–1114
25. Derome D, Griffa M, Koebel M, Carmeliet J (2011) Hysteretic swelling of wood at cellular scale probed by phase-contrast X-ray tomography. J Struct Biol 173:180–190
26. Steppe K, Cnudde V, Girard C, Lemeur R, Cnudde J-P, Jacobs P (2004) Use of X-ray computed microtomography for non-invasive determination of wood anatomical characteristics. J Struct Biol 148: 11–21
27. Viguié J, Dumont PJ, Mauret É, Du Roscoat SR, Vacher P, Desloges I, Bloch J-F (2011) Analysis of the hygroexpansion of a lignocellulosic fibrous material by digital correlation of images obtained by X-ray synchrotron microtomography: application to a folding box board. J Mater Sci 46:4756–4769
28. Antoine C, Nygård P, Gregersen ØW, Holmstad R, Weitkamp T, Rau C (2002) 3D images of paper obtained by phase-contrast X-ray microtomography: image quality

and binarisation. Nucl Inst Methods in Phys Res Sect A 490:392–402
29. Marulier C, Dumont P, Orgéas L, Caillerie D, du Roscoat SR (2012) Towards 3D analysis of pulp fibre networks at the fibre and bond levels. Nord Pulp Pap Res J 27:245–255
30. Rolland du Roscoat S, Decain M, Thibault X, Geindreau C, Bloch J-F (2007) Estimation of microstructural properties from synchrotron X-ray microtomography and determination of the REV in paper materials. Acta Mater 55:2841–2850
31. Samuelsen EJ, Gregersen OW, Houen P, Helle T, Raven C, Snigirev A (2001) Three-dimensional imaging of paper by use of synchrotron x-ray microtomography. J Pulp Pap Sci 27:50–53
32. Viguié J, Latil P, Orgéas L, Dumont P, Rolland du Roscoat S, Bloch J-F, Marulier C, Guiraud O (2013) Finding fibres and their contacts within 3D images of disordered fibrous media. Compos Sci Technol 89:202–210
33. Awal A, Rana M, Sain M (2015) Thermorheological and mechanical properties of cellulose reinforced PLA bio-composites. Mech Mater 80:87–95
34. Joffre T, Miettinen A, Wernersson EL, Isaksson P, Gamstedt EK (2014) Effects of defects on the tensile strength of short-fibre composite materials. Mech Mater 75:125–134
35. Rafsanjani A, Stiefel M, Jefimovs K, Mokso R, Derome D, Carmeliet J (2014) Hygroscopic swelling and shrinkage of latewood cell wall micropillars reveal ultrastructural anisotropy. J R Soc Interface 11:20140126
36. Avril S, Bonnet M, Bretelle A-S, Grédiac M, Hild F, Ienny P, Latourte F, Lemosse D, Pagano S, Pagnacco E (2008) Overview of identification methods of mechanical parameters based on full-field measurements. Exp Mech 48:381–402
37. Gamstedt EK, Bader TK, de Borst K (2013) Mixed numerical–experimental methods in wood micromechanics. Wood Sci Technol 47:183–202
38. Hill CA, Norton AJ, Newman G (2010) The water vapour sorption properties of Sitka spruce determined using a dynamic vapour sorption apparatus. Wood Sci Technol 44:497–514
39. Patera A, Derome D, Griffa M, Carmeliet J (2013) Hysteresis in swelling and in sorption of wood tissue. J Struct Biol 182:226–234
40. Harauz G, van Heel M (1986) Exact filters for general geometry three dimensional reconstruction. Proc IEEE Comput Vis Pattern Recognit Conf 146–156
41. Müller M, Czihak C, Vogl G, Fratzl P, Schober H, Riekel C (1998) Direct observation of microfibril arrangement in a single native cellulose fiber by microbeam small-angle X-ray scattering. Macromolecules 31:3953–3957
42. Batchelor WJ, Conn AB, Parker IH (1997) Measuring the fibril angle of fibres using confocal microscopy. Appita J 50:377–380
43. Donaldson L (1991) The use of pit apertures as windows to measure microfibril angle in chemical pulp fibers. Wood Fiber Sci 23:290–295
44. Leney L (1981) A technique for measuring fibril angle using polarized light. Wood Fiber Sci 13:13–16
45. Preston R (1934) The organization of the cell wall of the conifer tracheid. Philos Trans R Soc Lond Ser B 224:131–174
46. Fengel D (1969) The ultrastructure of cellulose from wood. Wood Sci Technol 3:203–217
47. Vincent L (1994) Morphological area openings and closings for grey-scale images. Proceedings of NATO Shape in Picture Workshop. Springer, Driebergen 197–208
48. Müller M, Burghammer M, Sugiyama J (2006) Direct investigation of the structural properties of tension wood cellulose microfibrils using microbeam X-ray fibre diffraction. Holzforschung 60:474–479
49. Bathe K-J (1996) Finite Element Procedures. Prentice Hall, Englewood Cliffs
50. Crisfield M, Galvanetto U, Jelenić G (1997) Dynamics of 3-D co-rotational beams. Comput Mech 20:507–519
51. Zienkiewicz OC, Taylor RL (2000) The finite element method: solid mechanics. Butterworth-Heinemann
52. Holzapfel GA (2000) Nonlinear Solid Mechanics. Wiley, Chichester
53. Krenk S (2009) Non-linear modeling and analysis of solids and structures. Cambridge University Press, Cambridge
54. Ji W, Waas AM, Bazant ZP (2013) On the importance of work-conjugacy and objective stress rates in finite deformation incremental finite element analysis. J Appl Mech 80:041024
55. Konnerth J, Buksnowitz C, Gindl W, Hofstetter K, Jäger A (2010) Full set of elastic constants of spruce wood cell walls determined by nanoindentation, Proceedings of the International Convention of the Society of Wood Science and Technology and United Nations Economic Commission for Europe—Timber Committee, Geneva
56. Cleveland WS, Loader C (1996) Smoothing by local regression: principles and methods, statistical theory and computational aspects of smoothing. Springer 10–49
57. Kajanto I, Niskanen K (1998) Dimensional stability. Teoksessa: Niskanen, K. (ed.), 222–259
58. Joffre T, Wernersson EL, Miettinen A, Luengo Hendriks CL, Gamstedt EK (2013) Swelling of cellulose fibres in composite materials: constraint effects of the surrounding matrix. Compos Sci Technol 74:52–59
59. Hult E-L, Larsson PT, Iversen T (2000) A comparative CP/MAS 13C-NMR study of cellulose structure in spruce wood and kraft pulp. Cellulose 7:35–55
60. Keylwerth R (1951) Formänderungen in Holzquerschnitten. Eur J Wood Wood Prod 9:253–260
61. Neagu RC, Gamstedt EK, Lindström, M (2005) Influence of wood-fibre hygroexpansion on the dimensional instability of fibre mats and composites. Compos Part A
62. Mazeau K, Rivet A (2008) Wetting the (110) and (100) surfaces of I_β cellulose studied by molecular dynamics. Biomacromolecules 9: 1352–1354
63. Rafsanjani A, Derome D, Wittel FK, Carmeliet J (2012) Computational up-scaling of anisotropic swelling and mechanical behavior of hierarchical cellular materials. Compos Sci Technol 72: 744–751
64. Almgren KM, Gamstedt EK, Berthold F, Lindström M (2009) Moisture uptake and hygroexpansion of wood fiber composite materials with polylactide and polypropylene matrix materials. Polym Compos 30:1809–1816